ATLAS NOTE

ATLAS-CONF-2011-035

March 21, 2011

Measurement of the top quark pair cross-section with ATLAS in pp collisions at $\sqrt{s}$ = 7 TeV in the single-lepton channel using b-tagging

The ATLAS Collaboration

Abstract

A measurement of the production cross-section for top quark pairs ($t\bar{t}$) in pp collisions at $\sqrt{s}$ = 7 TeV is presented using data recorded with the ATLAS detector at the Large Hadron Collider. Events are selected in the single-lepton (electron or muon) channel making use of the detector b-tagging capabilities. With a data sample of 35 pb^{-1} the inclusive top quark production cross-section is measured to be

$$\sigma_{t\bar{t}} = 186 \pm 10\,(\text{stat.})^{+21}_{-20}\,(\text{syst.}) \pm 6\,(\text{lumi.})\,\text{pb}.$$

Cross-check measurements are performed with kinematic fits of the reconstructed top mass and "cut and count" methods, and are found to be in good agreement with this result. The measurements agree with perturbative QCD calculations.

1 Introduction

A precise measurement of the top quark pair ($t\bar{t}$) production cross-section ($\sigma_{t\bar{t}}$) allows precision tests of perturbative QCD, whose predictions for $\sigma_{t\bar{t}}$ now have uncertainties at the level of 10%. In addition, $t\bar{t}$ production is an important background in various searches for physics beyond the Standard Model (SM), and new physics may also give rise to additional $t\bar{t}$ production mechanisms or modification of the top quark decay channels. Within the Standard Model, top quarks are predicted to decay to a W boson and a b-quark nearly 100% of the time, and the decay topologies are determined by the decays of the W bosons. The single-lepton and the dilepton modes, with branching ratios of 37.9% and 6.5% respectively, give rise to final states with one or two leptons, missing transverse energy and jets, some with b-flavour.

With a sample of 2.9 pb^{-1} taken with the Large Hadron Collider (LHC) at a centre of mass energy of $\sqrt{s}$ = 7 TeV, and using both the single-lepton and the dilepton decay channels, ATLAS measured the top quark production cross-section to be $\sigma_{t\bar{t}} = 145 \pm 31^{+42}_{-27}$ pb [1], in good agreement with the theoretical prediction $\sigma_{t\bar{t}} = 164.6^{+11.4}_{-15.7}$ pb, assuming a top mass of 172.5 GeV [2]. This note presents a measurement of the $t\bar{t}$ production in the single-lepton channel using 35 pb^{-1} of data taken during the 2010 run. The cross-section measurement is based on a fit to a discriminant built from several kinematic variables, and profits from the b-tagging capabilities of the detector. Alternative measurements using different discriminant variables and extraction methods are also presented. The baseline measurement is chosen to be the one with the smallest expected uncertainty. The main background contributions are determined using data-driven methods, since the theoretical uncertainties on the normalisation of these backgrounds are relatively large.

2 Detector, Data and Simulated Samples

The ATLAS detector [3] at the LHC covers nearly the entire solid angle[1] around the collision point. It consists of an inner tracking detector (ID) surrounded by a thin superconducting solenoid, electromagnetic and hadronic calorimeters, and an external muon spectrometer incorporating a large superconducting toroid magnet system. A three-level trigger system is used to select interesting events for recording and subsequent offline analysis. Only data for which all subsystems described above are fully operational are used in this analysis. Applying these requirements to $\sqrt{s}$ = 7 TeV pp collision data taken in stable beam conditions during the 2010 LHC run results in a data sample of 35 pb^{-1}. The luminosity value has a relative uncertainty of 3.4% [4].

Monte-Carlo (MC) simulation samples are used to develop and validate the analysis procedures, to calculate the acceptance for $t\bar{t}$ events and to evaluate the contributions from some background processes. After event generation, all samples are processed with the GEANT4 [5] simulation of the ATLAS detector [6], reconstructed and passed through the same analysis chain as the data. The same MC generator samples and associated systematic uncertainties as developed for the preceding $t\bar{t}$ cross-section measurement [1] are employed. However the detector simulation has been upgraded to reflect the improved knowledge of the detector material, alignment, geometry and calibration acquired since then.

The LHC instantaneous luminosity varied by several orders of magnitude during this data-taking period, reaching a peak of about 2.1×10^{32} cm^{-2}s^{-1}. At this luminosity an average of about four extra pp interactions are superimposed on each collision event. Pile-up corresponding on average to two extra events is added to the MC simulation. A small pile-up uncertainty is considered to cover the remaining mismatch in the observed number of reconstructed primary vertices between data and MC.

[1] In the right-handed ATLAS coordinate system, the pseudorapidity η is defined as $\eta = -\ln[\tan(\theta/2)]$, where the polar angle θ is measured with respect to the LHC beamline. The azimuthal angle ϕ is measured with respect to the x-axis, which points towards the centre of the LHC ring. The z-axis is parallel to the anti-clockwise beam viewed from above. Transverse momentum and energy are defined as $p_{\mathrm{T}} = p \sin\theta$ and $E_{\mathrm{T}} = E \sin\theta$, respectively.

3 Object Selection

The reconstruction of $t\bar{t}$ events makes use of electrons, muons, jets, and of missing transverse energy, which is an indicator of undetected neutrinos. The same object definition used for the previous $t\bar{t}$ cross-section measurement is used in this analysis, except for a tighter electron selection and more stringent ID track quality requirements for the muons. Electron candidates are defined as electromagnetic clusters consistent with the energy deposition of an electron in the calorimeters and with an associated well-measured track. They are required to satisfy $p_{\mathrm{T}} > 20$ GeV and $|\eta_{\mathrm{cluster}}| < 2.47$, where η_{cluster} is the pseudorapidity of the calorimeter cluster associated with the candidate. Candidates in the barrel to end-cap calorimeter transition region at $1.37 < |\eta_{\mathrm{cluster}}| < 1.52$ are excluded. Also, in order to suppress the background from photon conversions, the track must have an associated hit in the innermost pixel layer, except when the track passes through one of the 2% of pixel modules known to be dead. Muon candidates are reconstructed from track segments in the different layers of the muon chambers. These segments are combined starting from the outermost layer, with a procedure that takes material effects into account, and matched with tracks found in the inner detector. The final candidates are refitted using the complete track information from both detector systems, and required to satisfy $p_{\mathrm{T}} > 20$ GeV and $|\eta| < 2.5$.

To reduce background from leptons from the decays of hadrons and from heavy flavour decays inside jets, the leptons in each event are required to be "isolated". For electrons the E_{T} deposited in the calorimeter towers in a cone[2] of size $\Delta R = 0.2$ around the electron position is corrected to take into account the leakage of the electron energy. The remaining E_{T} is required to be less than 4 GeV. For muons, the corresponding calorimeter isolation energy in a cone of $\Delta R = 0.3$ is required to be less than 4 GeV, and the analogous sum of track transverse momenta in a cone of $\Delta R = 0.3$ is also required to be less than 4 GeV. Additionally, muons are required to have a distance ΔR greater than 0.4 from any jet with $p_{\mathrm{T}} > 20$ GeV, further suppressing muons from heavy flavour decays inside jets.

Jets are reconstructed with the anti-k_t algorithm [7] ($\Delta R = 0.4$) from topological clusters [8] of energy deposits in the calorimeters, calibrated at the electromagnetic scale appropriate for the energy deposited by electrons or photons. These jets are calibrated to the hadronic energy scale, using a correction factor which depends upon p_{T} and η obtained from simulation. If the closest object to an electron candidate is a jet with a separation $\Delta R < 0.2$ the jet is removed to avoid double-counting of electrons as jets.

Jets stemming from the hadronisation of b-quarks are identified using two complementary tagging algorithms that take advantage of the long lifetime of b-hadrons (about 1.5 ps). The first algorithm, called JetProb [9] and used for the baseline analysis reported here, relies on the transverse impact parameter d_0 of the tracks in the jet: this is the distance of closest approach in the transverse plane of a track to the primary vertex. It is signed with respect to the jet direction: the sign is positive if the track crosses the jet axis in front of the primary vertex, negative otherwise. The signed impact parameter significance, d_0/σ_{d_0}, of each selected track is compared to a resolution function for prompt tracks, to measure the probability that the track originates from the primary vertex. The individual track probabilities are then combined into a probability that the jet originates from the primary vertex. Different resolution functions are used for experimental data and for simulated data, to account for small residual discrepancies. This algorithm can reach very high tagging efficiency, though at a cost of a modest rejection of light jets: in simulated $t\bar{t}$ events for a 70% b-tagging efficiency about 5% of the light jets are wrongly tagged. The second algorithm, called SV0 [10], attempts to reconstruct the inclusive vertex formed by the decay products of the bottom hadron and possibly subsequent charm hadron decay products. The discriminating variable for SV0 is the decay length significance, $L_{3D}/\sigma_{L_{3D}}$, measured in 3D and signed with respect to the jet direction. The SV0 operating point chosen requires that $L_{3D}/\sigma(L_{3D}) > 5.85$, yielding in simulated $t\bar{t}$ events a 50% tagging efficiency for b-jets and a mistagging efficiency for light jets less than 0.4%.

The b-tagging efficiencies and mistag fractions for the two tagging algorithms at the various operat-

[2] $\Delta R = \sqrt{(\Delta\eta)^2 + (\Delta\phi)^2}$

ing points used have been measured in data. The efficiency measurement is based on a sample of jets containing muons, and makes use of the transverse momentum of the muon relative to the jet axis. The measurement of the mistag fractions is performed on an inclusive jet sample and relies on two methods, one which uses the invariant mass spectrum of tracks associated to reconstructed secondary vertices to separate light- and heavy-flavour jets, and one based on the rate at which secondary vertices with negative decay-length significance are present in data. These measurements are provided in the form of p_{T}-dependent scale factors correcting the b-tagging performance in simulation to that observed in data. For a b-tagging efficiency around 50% with either the JetProb or the SV0 algorithms, the scale factor for efficiency is rather constant and close to 0.9 ± 0.1. For a typical jet of $p_{\mathrm{T}} = 50$ GeV, the simulation underestimates the mistagging efficiency of light jets with SV0 by factors of 1.0±0.2 and 1.2±0.2 for $|\eta| < 1.2$ and $1.2 < |\eta| < 2.5$, respectively. With JetProb operating at the same point, the scale factor for mistags in the central region is 1.3±0.4, while it is measured to be 1.1±0.2 at a 70% tagging efficiency.

The missing transverse energy $E_{\mathrm{T}}^{\mathrm{miss}}$ is constructed from the vector sum of calorimeter energy deposits, resolved into the transverse plane. Cells not associated to muons, electrons with $p_{\mathrm{T}} > 10$ GeV, photons, taus, jets and soft jets are included at the EM scale. The electrons, muons and jets used in the $E_{\mathrm{T}}^{\mathrm{miss}}$ calculation are used consistently with the definitions stated above.

4 Treatment of Backgrounds

The main expected backgrounds in the single-lepton channel are W+jets, which can give rise to the same final state as $t\bar{t}$ signal, and QCD multi-jet events. The latter only contribute to the signal selection if the reconstructed $E_{\mathrm{T}}^{\mathrm{miss}}$ is sufficiently large and a fake lepton is reconstructed. Fake leptons originate in misidentified jets or are non-prompt leptons from semileptonic decays of bottom or charm quarks.

For the baseline analysis in which the JetProb b-tagging probability of the jets is used as an input of the fit, both W+jets and QCD multi-jet backgrounds are dominated by events with light quarks and gluons. The shape of the QCD multi-jet background is determined with data-driven methods, the matrix method for the muon channel and the fitting method for the electron channel, summarized in [11]. The Monte-Carlo simulation is expected to predict correctly the W+jet kinematical distributions, but not the relative normalisations of the different jet multiplicities. Therefore the fit employs six different W+jet templates, each with its individual fit parameters. Independent Gaussian constraints on the W+jet normalisation in each bin, based on the Berends-Giele scaling described in [1], are applied. Since Z+jet is a much smaller background, a single template is used. The shapes of the other sources of background (single top, diboson) are obtained from Monte-Carlo simulation, and the templates are normalized to the latest next to leading order (NLO) calculations of the respective cross-sections.

All the other analyses used as cross-checks, in addition to using the zero tag samples, explicitly require some jets to be b-tagged by the SV0 algorithm. Therefore light-quark and gluon final states are strongly suppressed and their contribution becomes comparable to those with $b\bar{b}$ pairs, $c\bar{c}$ pairs and single c quarks, which are all of a similar magnitude. The QCD multi-jet background is estimated using the same techniques described in [11] after the b-tagging algorithm is applied. For the muon channel, the same 30% systematic uncertainty as described in [11] applies, except for events with two b-tags which are statistically limited and where the uncertainty is approximately 100%. In the electron channel, the technique tends to be more statistically limited and the uncertainties are typically 100% for events with one b-tag and 150% for events with two b-tags. These uncertainties represent the starting point and are not fixed in the fit, as will be explained in Section 6.

5 Event Selection

The single-lepton $t\bar{t}$ final state is characterized by an isolated lepton with relatively large p_{T}, missing transverse energy corresponding to the neutrino from the leptonic W decay, two b-quark jets and two light jets from the hadronic W decay. The event selection follows closely the one used in [1] except for the different $E_{\mathrm{T}}^{\mathrm{miss}}$ and transverse leptonic W mass requirements, depending on whether the electron or the muon channel is considered. Events are triggered by a single-lepton trigger. The electron trigger requires a level-1 electromagnetic cluster with $p_{\mathrm{T}} > 10$ GeV. A more refined electromagnetic cluster selection is required in the level-2 trigger, and a match between the selected calorimeter electromagnetic cluster and an inner detector track is required in the event filter. The muon trigger requires a $p_{\mathrm{T}} > 10$ GeV track in the muon trigger chambers at level-1, matched by a muon of $p_{\mathrm{T}} > 13$ GeV reconstructed in the precision chambers and combined with an inner detector track at the event filter. Leptons which pass the offline selection are well within the plateau region of the trigger turn-on curves.

After the trigger, the event is required to contain one and only one reconstructed lepton with $p_{\mathrm{T}} > 20$ GeV, matching the corresponding high-level trigger object. Selected events must have at least one offline-reconstructed primary vertex with at least five tracks, and events are discarded if any jet with $p_{\mathrm{T}} > 20$ GeV is identified as out-of-time activity or calorimeter noise. To reject a significant fraction of the QCD multi-jet background, the $E_{\mathrm{T}}^{\mathrm{miss}}$ is required to be larger than 35 (20) GeV in the electron (muon) channel. Further rejection is achieved by requiring the transverse leptonic W mass to be larger than 25 GeV (60 GeV - $E_{\mathrm{T}}^{\mathrm{miss}}$) in the electron (muon) channel. Finally, the event is required to have one or more jets with $p_{\mathrm{T}} > 25$ GeV and $|\eta| < 2.5$, these values being a compromise between the efficiency of the $t\bar{t}$ selection and the rejection of W+jets and QCD multi-jet background. Events are then classified by the number of jets fulfilling these requirements that they contain and by their lepton flavour.

Table 1 shows the number of selected events in the different jet multiplicities, together with the expectations from the different Standard Model processes, obtained from Monte-Carlo simulation except the QCD contribution which is obtained using data-driven methods as explained in the previous section.

Table 1: Selected events in the electron (top) and muon (bottom) channels split up according to jet multiplicity. The uncertainties quoted are statistical and systematic.

Electron Channel	1 jet	2 jets	3 jets	4 jets	≥ 5 jets
$t\bar{t}$	14.3 ± 2.9	61 ± 9	116 ± 13	111 ± 16	82 ± 12
W+jets	9000 ± 1900	2300 ± 700	580 ± 250	140 ± 90	41 ± 26
QCD multijets	290 ± 140	123 ± 62	62 ± 31	13 ± 7	8 ± 4
Single Top	36 ± 4	42 ± 5	22 ± 4	7.8 ± 1.8	3.1± 0.7
Z+jets	65 ± 14	62 ± 20	32 ± 14	12 ± 8	6 ± 4
Diboson	35.3 ± 2.8	30.1 ± 2.4	9.3 ± 1.5	2.2 ± 0.5	0.4± 1
Total Predicted	9400 ± 1900	2700 ± 800	830 ± 250	290 ± 90	141 ± 29
Data Observed	9481	2552	781	273	127
Muon Channel	1 jet	2 jets	3 jets	4 jets	≥ 5 jets
$t\bar{t}$	19 ± 4	81 ± 12	161 ± 18	158 ± 22	115 ± 16
W+jets	19000 ± 4000	4600 ± 1500	1100 ± 500	250 ± 150	70 ± 40
QCD multijets	520 ± 160	287 ± 86	121 ± 36	30 ± 10	20 ± 6
Single Top	57 ± 7	64 ± 8	32 ± 6	11.1± 2.5	4.0± 0.9
Z+jets	770 ± 160	250 ± 80	69 ± 30	19 ± 12	6 ± 4
Diboson	63 ± 5	55 ± 4	16.1 ± 2.6	3.4± 0.7	0.6± 0.1
Total Predicted	20000 ± 4000	5300 ± 1500	1500 ± 500	470 ± 160	210 ± 50
Data Observed	20583	5228	1356	448	205

6 Baseline Multivariate Analysis

The baseline analysis is based on a multivariate likelihood discriminant D, constructed from the following four input variables:

- The pseudorapidity of the lepton.
- The aplanarity, defined as 1.5 times the smallest eigenvalue of the momentum tensor $M_{ij} = \sum_{k=1}^{N_{\text{objects}}} p_{ik} p_{jk} / \sum_{k=1}^{N_{\text{objects}}} p_k^2$, where p_{ik} is the i-th momentum component and p_k is the modulus of the momentum of object k. To smooth the aplanarity distribution $\exp(-8 \times \text{aplanarity})$ is used as input to the discriminant.
- The variable $H_{T,3p}$, given by the transverse energy of all jets except the two leading ones, normalized to the sum of absolute values of all longitudinal momenta in the event, $H_{T,3p} = \sum_{i=3}^{N_{\text{njets}}} |p_{\text{T},i}^2| / \sum_{j=1}^{N_{\text{objects}}} |p_{z,j}|$, where p_{T} is the transverse momentum and p_z the longitudinal momentum. The sum over all objects includes the charged lepton, the neutrino and all jets. The longitudinal momentum of the neutrino is obtained by solving the event kinematics using the W mass constraint and taking the smaller neutrino p_z solution. To smooth the $H_{T,3p}$ distribution $\exp(-4 \times H_{T,3p})$ is used as input to the discriminant.
- The average of the two lowest light-jet probabilities (P_l) in the event, as computed by the JetProb b-tagging algorithm (see Section 3). These are the jets which have the most significant b-tags. The weight returned by the tagger is transformed to $W_{JP} = -\log_{10} P_l$.

The choice of variables is intended to be complementary in terms of sensitivity and uncertainties while the small number of variables is intended to maintain simplicity.

To provide the maximum sensitivity, the fit is performed simultaneously to three samples (3-jet, 4-jet and ≥5-jet) in the electron and muon channels separately. The high jet-multiplicity bins are the ones where one expects to collect most of the $t\bar{t}$ signal, as seen in Table 1. However, there is also a significant fraction of signal in the three-jet bin, which is included in the fit. Furthermore, the inclusion of the three-jet bin helps to constrain the systematic uncertainty due to the W+jets modeling. Figures 1 and 2 show some distributions of the templates for the selected data superimposed on the Standard Model prediction.

The discriminant D is a projective likelihood estimator without prior decorrelation of the input variables. The cross-section is extracted from a binned likelihood fit of D to a weighted sum of templates corresponding to the signal and different backgrounds. The template shape describing $t\bar{t}$ events is taken from simulation, as are the shapes describing W+jets, Z+jets, single top and di-boson processes. The $t\bar{t}$ signal templates across the six channels are assumed to be 100% correlated. Their normalisation is the parameter of interest in the fit and is allowed to vary freely. The fit employs six different templates for W+jets, each with its individual normalization parameter obtained from simulation, and a 24 (40, 60)% Gaussian constraint on the 3-jet (4-jet, ≥5-jet) bin is applied. As the Z+jets constitutes a small background, 100% correlation is assumed across the six channels and a single template is used. Its normalisation is constrained to be within 30% of its nominal value. The small contributions from single top and diboson production are normalized to the latest NLO calculation of their respective cross-sections [12, 13]. These calculations have uncertainties of approximately 10% for single top and 5% for diboson production, which are used as Gaussian constraints on their normalisation. Finally, six independent parameters are used for the QCD multijet channels, assuming a 50% uncertainty in their normalisation [11].

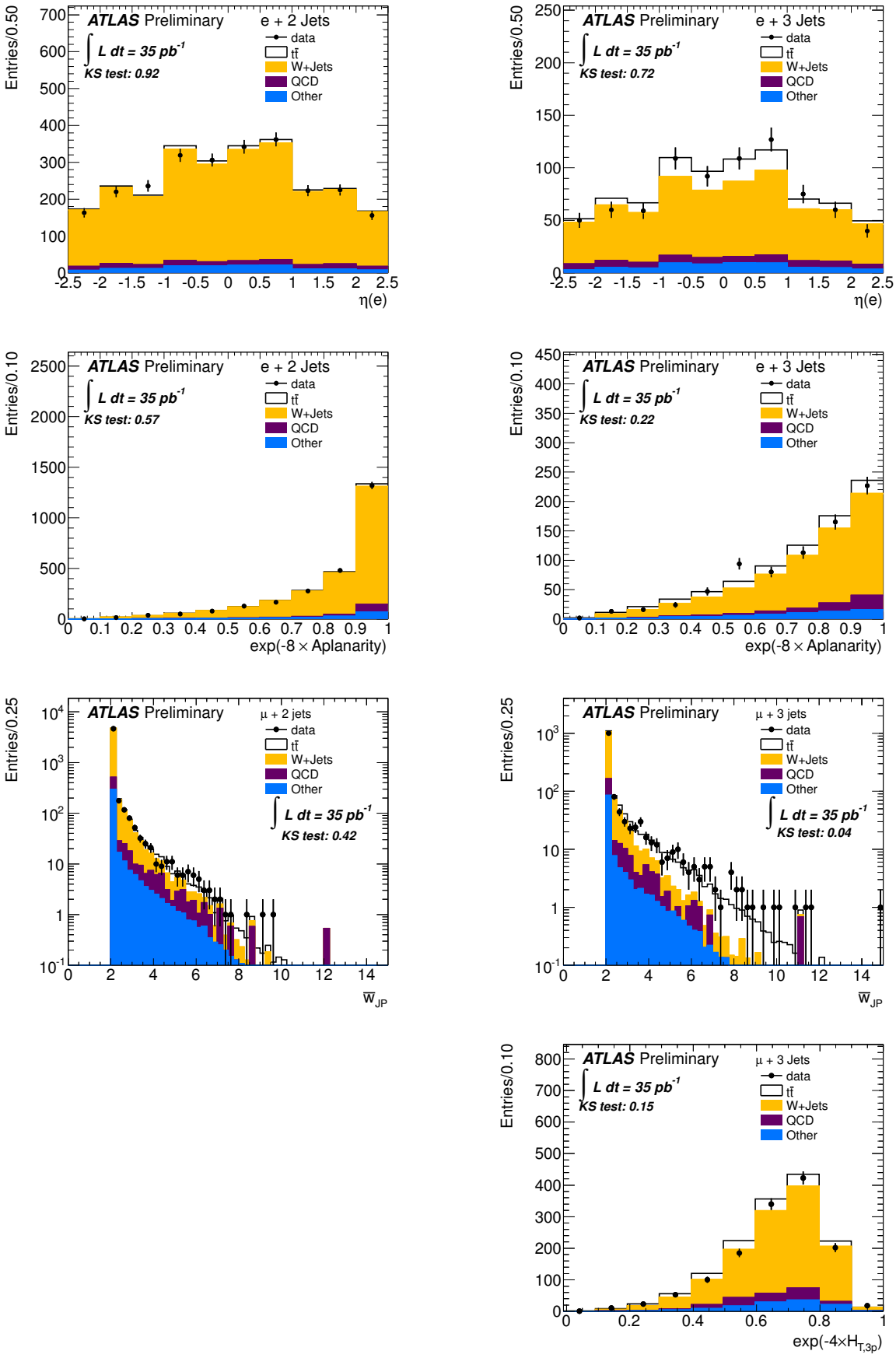

(a) 2-jet (b) 3-jet

Figure 1: Distribution of the electron pseudorapidity (top row) and aplanarity (second row) in the electron channel, and of jet probability (third row) and $H_{T,3p}$ (bottom row) in the muon channel for the 2-jet sample (a) and the 3-jet sample (b). $H_{T,3p}$ is not shown in the 2-jet channel as it requires at least three jets to be computed. Data are superimposed on the Standard Model expectation normalized according to the result of the fit. Kolmogorov-Smirnov (KS) tests between the data and the predictions are shown.

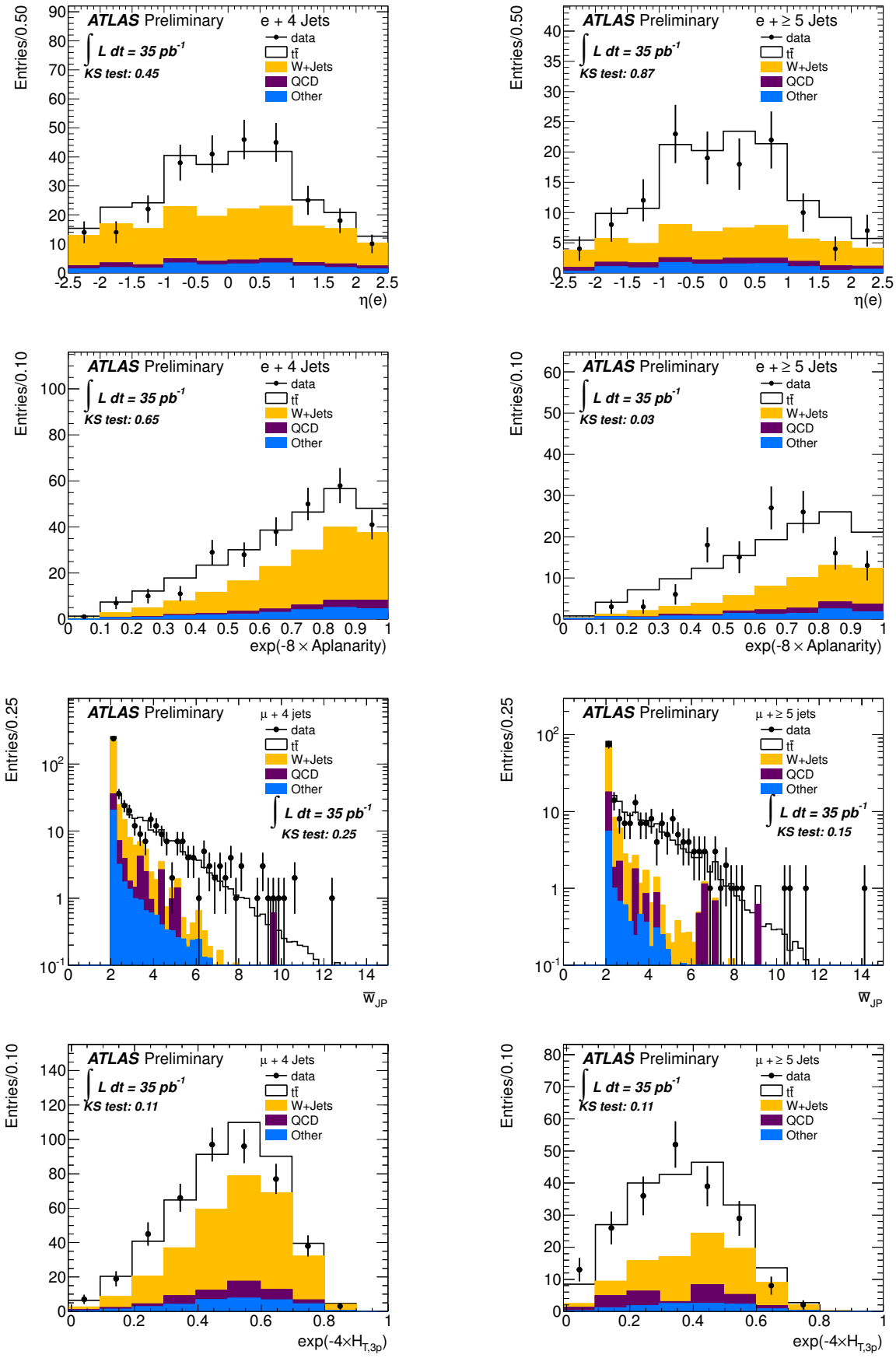

(a) 4-jet (b) ≥5-jet

Figure 2: Distribution of the electron pseudorapidity (top row) and aplanarity (second row) in the electron channel, and of jet probability (third row) and $H_{T,3p}$ (bottom row) in the muon channel for the 4-jet sample (a) and ≥5-jet sample (b). Data are superimposed on the Standard Model expectation normalized according to the result of the fit. Kolmogorov-Smirnov (KS) tests between the data and the predictions are shown.

A profile likelihood in which systematic variations are not simply used to test the bias of the fit, but enter directly in the minimisation process as parameters of the fit [14] is used. Nuisance parameters for most systematic uncertainties are added to the fit. The nuisance parameters adjust the size of the corresponding systematic uncertainties, and their fitted values correspond to the amount that best fits the data, allowing the fit to effectively check and constrain those uncertainties using the data itself. Each nuisance parameter is assumed to be Gaussian-distributed with mean value zero. A nuisance parameter fitted value of one corresponds to the variation given in the input for the corresponding systematic uncertainty. The uncertainty of the nuisance parameter fitted value determines the range in which the variation of the systematic uncertainty is compatible with the data with a 68% confidence level.

Many sources of systematic uncertainties have been considered. The uncertainties due to Monte-Carlo simulation modeling of the lepton trigger, reconstruction and selection efficiencies have been assessed using tag and probe techniques on $Z \rightarrow$ ee and $Z \rightarrow \mu\mu$ events selected from the same data sample used for the $t\bar{t}$ analyses. Electron trigger and reconstruction efficiencies in simulation were found to be consistent with data within 1.5%, but a discrepancy at the level of 3.5% was found in the identification efficiency. For muons, the product of reconstruction and identification efficiencies is consistent in data and simulation within 1%, but there is a few percent discrepancy in specific regions for the trigger efficiency. The simulation was made to agree with the data for both electrons and muons by applying efficiency scale factors as multiplicative event weights. The accuracy of lepton momentum scale and resolution in simulation was checked using reconstructed distributions of the Z mass. They were found to be quite consistent with data, and remaining disagreements were corrected for by rescaling and smearing the momentum of the lepton.

The jet energy scale (JES) and its uncertainty have been derived combining information from test-beam data, LHC collision data, and simulation, and varies in the range 4–8% as a function of jet p_{T} and η. Since the selected data have been split into three subsamples according to the jet multiplicity (3-, 4- and ≥5-jet,) the fit is able to constrain the JES just by counting the number of jets that pass the p_{T} threshold. It is estimated that jet energy resolution in data and simulation agree within 10%, which has been taken as the systematic uncertainty. Jet reconstruction efficiency is reproduced by the simulation within 2% and is also taken into account as a systematic uncertainty.

To estimate the effect of shape uncertainties on the main backgrounds, the QCD templates have been replaced with alternative data-driven templates, keeping their normalisation identical to the nominal one. Similarly, the W+jets templates have been modified by varying the ALPGEN [15] generator settings. The heavy flavour content of W+jets samples has been assessed in the 1- and 2-jet bins by studying the secondary vertex mass and the number of tags. The theoretical uncertainties on the extrapolation of these measurements to the signal region have been studied by varying the relevant ALPGEN parameters. The studies result in uncertainties of 70%, 90% and 110% in the 3-, 4- and ≥ 5-jet samples, respectively.

The uncertainty due to the amount of initial and final state radiation (ISR,FSR) in $t\bar{t}$ events is assessed using AcerMC [16] Monte-Carlo samples generated with either more or less ISR or FSR. To quantify the uncertainty due to the choice of the signal Monte-Carlo generator, the default MC@NLO [17] is replaced by POWHEG [18] hadronized with either HERWIG [19] or PYTHIA [20]. Uncertainties in the parton distribution functions (PDF) have been considered following the prescription in [21]. Finally, the uncertainty derived from the simulation of pile-up in the Monte-Carlo samples has been taken into account by using reweighted templates such that the number of reconstructed primary vertices per event, which is taken as a measure of the pile-up amount, matches the one found in data.

Since no cut on the JetProb b-tagging probability w_{JP} is applied, the analysis is only sensitive to variations in the shape of the JetProb probability distribution. By combining individual scale factors SF_i defined for JetProb at two operating points (for example $w_{JP} < w_i$), new scale factors SF_{ij} for jets with $w_j < w_{JP} < w_i$ are defined, allowing rescaling of the complete distribution. The corresponding uncertainties are evaluated by varying the tagging and mistag probabilities at the two working points

independently within their respective uncertainties, conservatively assuming that they are uncorrelated. The magnitudes of these four variations are used as nuisance parameters in the final fit.

The influence of the most important parameters on the cross-section has been studied with ensemble tests of 1000 pseudo-experiments (PE). In these PE the nominal normalisations are used, and random variations of all nuisance parameters within their $\pm 1\sigma$ ranges are applied. When all systematic uncertainties are included, the expected uncertainty, including template statistics, amounts to 11.5%. When the fits are repeated without any nuisance parameters, the uncertainty is reduced to 5.2%, which corresponds to the statistical uncertainty. Subtracting this number from the full uncertainty results in an expected systematic uncertainty of 10.3%. Table 2 shows the complete set of measured systematic uncertainties. Table A.1 in Appendix A shows the fitted nuisance parameters.

Table 2: Results of the profile likelihood fit to muon and electron data. The relative statistical and systematic uncertainties for 35 pb^{-1} are shown. Each systematic uncertainty is obtained as the difference in quadrature between the total uncertainty and the uncertainty obtained after having fixed the corresponding nuisance parameter to its fitted value.

Statistical Error (%)	**+5.3**	**-5.2**
Object selection (%)		
Jet energy scale	+3.8	-2.8
Jet reconstruction efficiency	+4.2	-4.2
Jet energy resolution	+0.8	-0.2
Electron scale factor	+1.2	-0.8
Muon scale factor	+0.5	-0.6
Electron smearing	+0.3	-0.2
Muon smearing	+0.6	-0.4
Background modeling (%)		
Wjets HF content	+7.2	-6.3
Wjets shape	+1.5	-1.5
QCD shape	+1.0	-1.0
$t\bar{t}$ signal modeling (%)		
ISR/FSR	+4.0	-4.0
NLO generator	+0.5	-0.7
Hadronisation	+0.0	-0.6
PDF	+1.7	-1.7
Others (%)		
b-tagging calibration	+7.5	-6.3
Simulation of pile-up	+1.5	-0.6
Templates statistics	+1.6	-1.5
Total Systematic (%)	**+11.5**	**-10.5**

The linearity of the fit as a function of the input $t\bar{t}$ cross-section has been checked. For each of nine cross-section values between 120 pb and 200 pb 1000 PE have been generated. All templates are normalized to their nominal values except for $t\bar{t}$, whose initial normalisation is adjusted according to the input cross-section. As shown in Fig. 3 (a) the fit shows good linearity over the full range. The uncertainty returned by the fitter can be checked against the uncertainty from ensemble testing via pull distributions, shown in Fig. 3 (b).

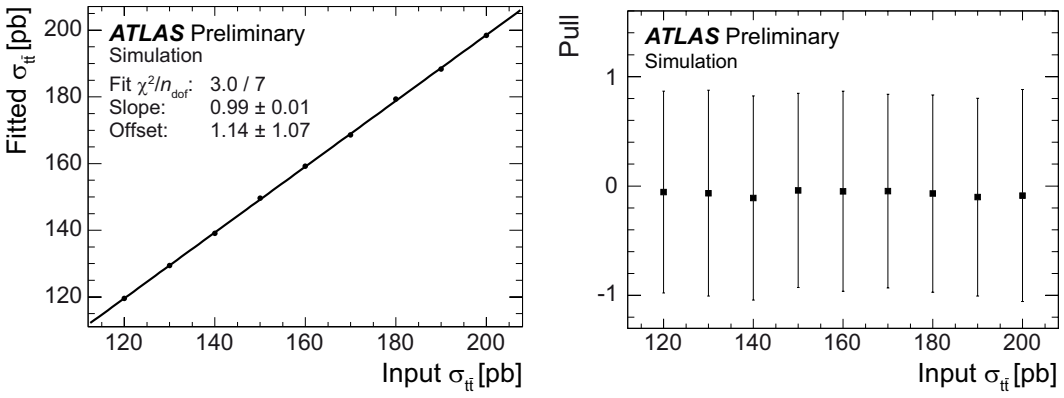

(a) Linearity

(b) Pull

Figure 3: (a) Linearity test and (b) pull distribution as a function of input $t\bar{t}$ cross-section.

The pull distributions are slightly smaller than unity[3]. This indicates that the PE do not include a small part of the uncertainty that the likelihood fitter detects. To be conservative, all quoted numbers are based on the larger uncertainties obtained from the likelihood fitter. The robustness of this fitting approach has also been checked with ensemble tests. Pseudo-experiments are performed from various distributions that correspond to extreme parameter choices or that do not match the original ones. The latter include templates distorted within the envelope of the systematic uncertainties and templates obtained applying systematic shifts to the distributions found in data. The variations in the fitted $t\bar{t}$ cross-section are well within the quoted systematic uncertainties. Furthermore, the likelihood is "profiled" by fixing the value of the $t\bar{t}$ cross-section and minimizing with respect to all other fit parameters. The fitted values of all parameters change smoothly according to their correlations with the $t\bar{t}$ cross-section.

The maximum likelihood fit including all systematic uncertainties and bin-by-bin statistical uncertainties of the templates is applied to the data to extract the $t\bar{t}$ production cross-section:

$$\sigma_{t\bar{t}} = 186 \pm 10\,(\text{stat.})^{+21}_{-20}\,(\text{syst.}) \pm 6\,(\text{lumi.})\,\text{pb}.$$

Figure 4 shows the the likelihood discriminant distribution D for the selected data superimposed on the prediction. The fitter treats the templates of the six analysis channels with 20 bins each as one large 120-bin histogram, the left bins corresponding to the muon channel and the right bins to the electron channel. The expected contributions have been scaled according to the results of the fit.

[3]The average pull width over the range of input cross-sections considered in Fig. 3 is 0.92 ± 0.01.

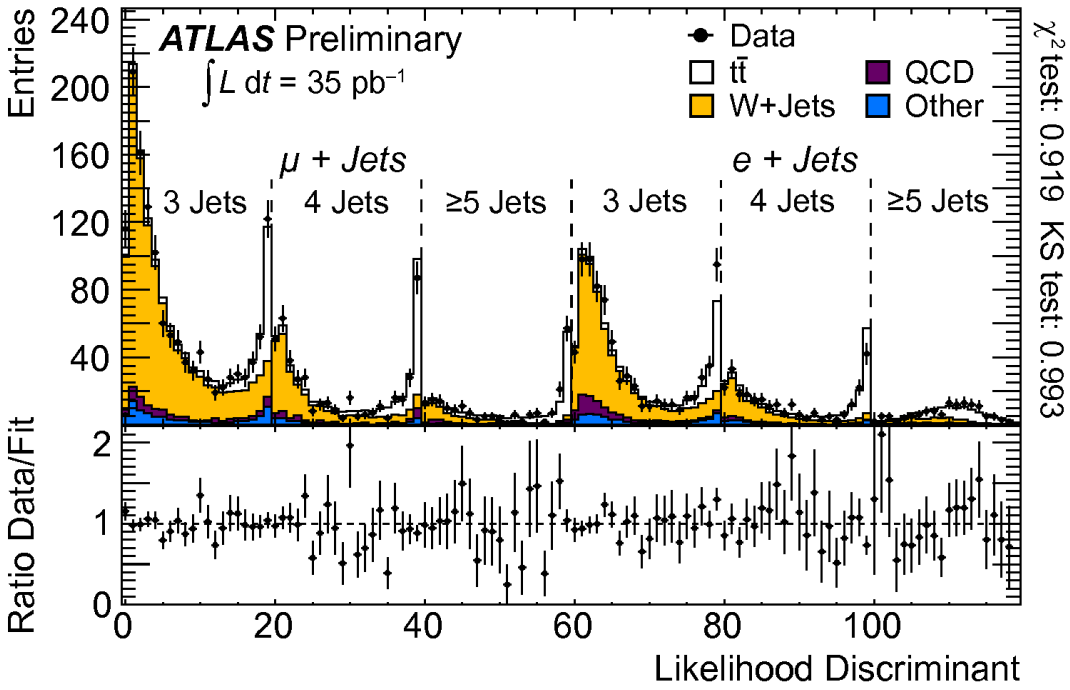

Figure 4: (Top) D distribution of data superimposed on expectations, scaled to the results of the fit. The left bins correspond to the muon channel and the right bins to the electron channel. (Bottom) The ratio of data to fit result.

7 Cross-Check Analyses with b-tagging Cuts

All other analyses used as cross-checks require that at least one jet be identified as a b-jet with the SV0 algorithm. Figure 5 shows the distribution of the number of b-tags in the electron and muon channels after the selection presented in Section 5 is applied, for events containing four or more jets. The uncertainties shown as hatched areas correspond only to the background prediction.

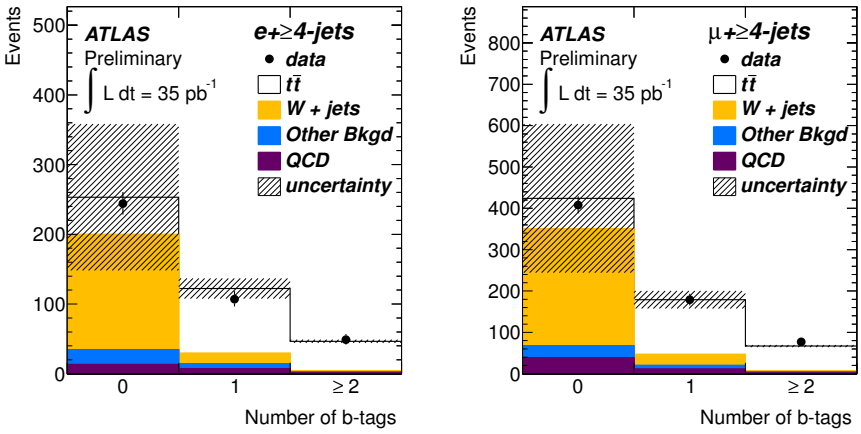

Figure 5: Distribution of the number of tagged jets in events passing the selection in the electron channel (left) and the muon channel (right). The data are shown by the solid points, compared to the sum of all expected contributions, taken from simulations ($t\bar{t}$ signal, single top, W and Z+jets) or estimated using a data-driven technique (QCD multi-jet). The hatched area shows the uncertainty on the total expectation due to the uncertainties on the background estimates.

7.1 Cross-section from counting

The simplest approach to a measurement of the $t\bar{t}$ cross-section consists of estimating the yield of signal events (N_{sig}) in the tagged 4-jet sample, which is calculated by subtracting the estimated background (N_{bkg}) from the observed event yield (N_{obs}). The $t\bar{t}$ cross-section is extracted using the formula:

$$\sigma(t\bar{t}) = \frac{N_{sig}}{\int L\,dt \times \epsilon} = \frac{N_{obs} - N_{bkg}}{\int L\,dt \times \epsilon}$$

where $\int L\,dt$ is the integrated luminosity and ϵ is the product of the signal acceptance, efficiency and branching ratio, estimated from simulation. For the QCD multi-jet background, the data-driven techniques already mentioned are used. The estimation of the W+jet background is based on the W/Z ratio as described in [11]. The per-event b-tagging probability is subsequently folded in as explained in [1]. For the expected background coming from Z+jets and single top production, simulation estimates are used. Table 3 lists the estimated signal and background contributions used in this calculation. The W+jets background is reduced by an order of magnitude with respect to the analysis without b-tagging [11].

Table 3: Estimated yield of signal and background events in the b-tagged 4-jet inclusive sample for electrons and muons. The uncertainty on the background estimates includes all sources of uncertainties. The uncertainty on the estimated number of signal events include both the background uncertainty and the statistical uncertainty on the number of observed events. The $t\bar{t}$ estimate shown is the difference between the observed count and the background estimate.

	e+jets	μ+jets
Data Observed	156	246
W+jets estimate	12 ± 5	40 ± 14
Total background estimate	29 ± 11	64 ± 15
$t\bar{t}$ estimate	127 ± 17	182 ± 22

The three largest contributions to the systematic uncertainty on the estimated signal acceptance are the b-tagging efficiency (11%), the jet energy scale (9%), and the ISR/FSR (7%). The electron and muon channels are combined using binned profile likelihood fits of the estimated number of events to data, where the bin contents are modeled by Poisson distributions and the systematic uncertainties are included as gamma distribution constraints on the parameters of the fit. The resulting combined cross-section is: $\sigma_{t\bar{t}} = 156 \pm 10$ (stat.) $^{+34}_{-28}$ (syst.) ± 6 (lumi.) pb.

7.2 Fit of the 3-jet invariant mass in the 3-, 4-, and $\geq$ 5-jet samples

For this top mass profile fit analysis, the same profile likelihood technique used for the baseline analysis is used to fit the three-jet invariant mass m_{jjj} distribution of candidate hadronic top decays, defined as the combination of three jets having the highest vector sum p_{T} , in the selected data sample ($\mathcal{D}_{data}$) to a weighted sum of templates corresponding to $t\bar{t}$ ($\mathcal{D}_{t\bar{t}}$), W+jets ($\mathcal{D}_{W}$), QCD ($\mathcal{D}_{QCD}$), and the rest of physics backgrounds ($\mathcal{D}_{other}$) (single top, Z+jets, and di-boson): $\mathcal{D}_{data} = k_{t\bar{t}} \times \mathcal{D}_{t\bar{t}} + \beta_{W+jets} \times \mathcal{D}_{W} + \beta_{QCD} \times \mathcal{D}_{QCD} + \beta_{other} \times \mathcal{D}_{other}$.

The template shape for the QCD multi-jet background has been obtained from the data-driven methods as explained for the baseline analysis. However, to avoid statistical fluctuations after tagging, the events before tagging were reweighted to take into account the average probability for a jet to be tagged. This jet tagging rate is a 2D function of the jet p_{T} and η and is measured in data in an orthogonal sample of events. The W+jets shape is taken from simulation, but it is first validated by comparing the prediction from simulation to data in a control sample.

The $k_{t\bar{t}}$ and β_i factors multiply the nominal cross-section from Standard Model predictions implemented in the simulation. The $k_{t\bar{t}}$ and β_{W+jets} scaling factors are fitted simultaneously and the nominal SM prediction would correspond to a scaling factor of one. The factor β_{QCD} is set such as to reproduce the number of QCD events predicted by the data-driven method (Section 4) in each channel. The coefficient β_{other} is set to one, corresponding to the SM expectation. The uncertainties on the β_{QCD} and β_{other} factors are propagated to the final result of the fit and the corresponding systematics evaluated.

Considering all sources of systematic uncertainties outlined in the previous section, we fit the data simultaneously on nine samples for the electron channel, and nine samples for the muon channel: 3-, 4- and $\geq$ 5-jet and 0-, 1- and $\geq$ 2-tag. The expected statistical and systematic uncertainties, evaluated using pseudoexperiments, are found to be $\pm$5.3% and $\pm$11.2% respectively. The most important contributions to the total systematic uncertainty are the uncertainties on the b-tagging fraction (7.5%) and on the jet reconstruction efficiency (5.1%). The resulting $t\bar{t}$ cross-section is measured to be $\sigma_{t\bar{t}} = 156 \pm 8\,(\mathrm{stat.})^{+18}_{-16}\,(\mathrm{syst.}) \pm 5\,(\mathrm{lumi.})$ pb. The systematic uncertainties that have been most significantly constrained by the fit are $t\bar{t}$ modeling, b-tagging, W+jets shape and jet energy scale. Figure 6 presents the results of the fit: the 3-jet invariant mass distributions for the 3-, 4- and $\geq$ 5-jet and 0-, 1- and $\geq$ 2-tag selected data in the muon channel are shown together with the predictions. The $t\bar{t}$ and W+jets contributions have been scaled according to the results of the fit and the shapes of the Monte-Carlo samples morphed in accordance with the results of the nuisance factors. Figure B.1 in Appendix B shows the result of the fit in the electron channel.

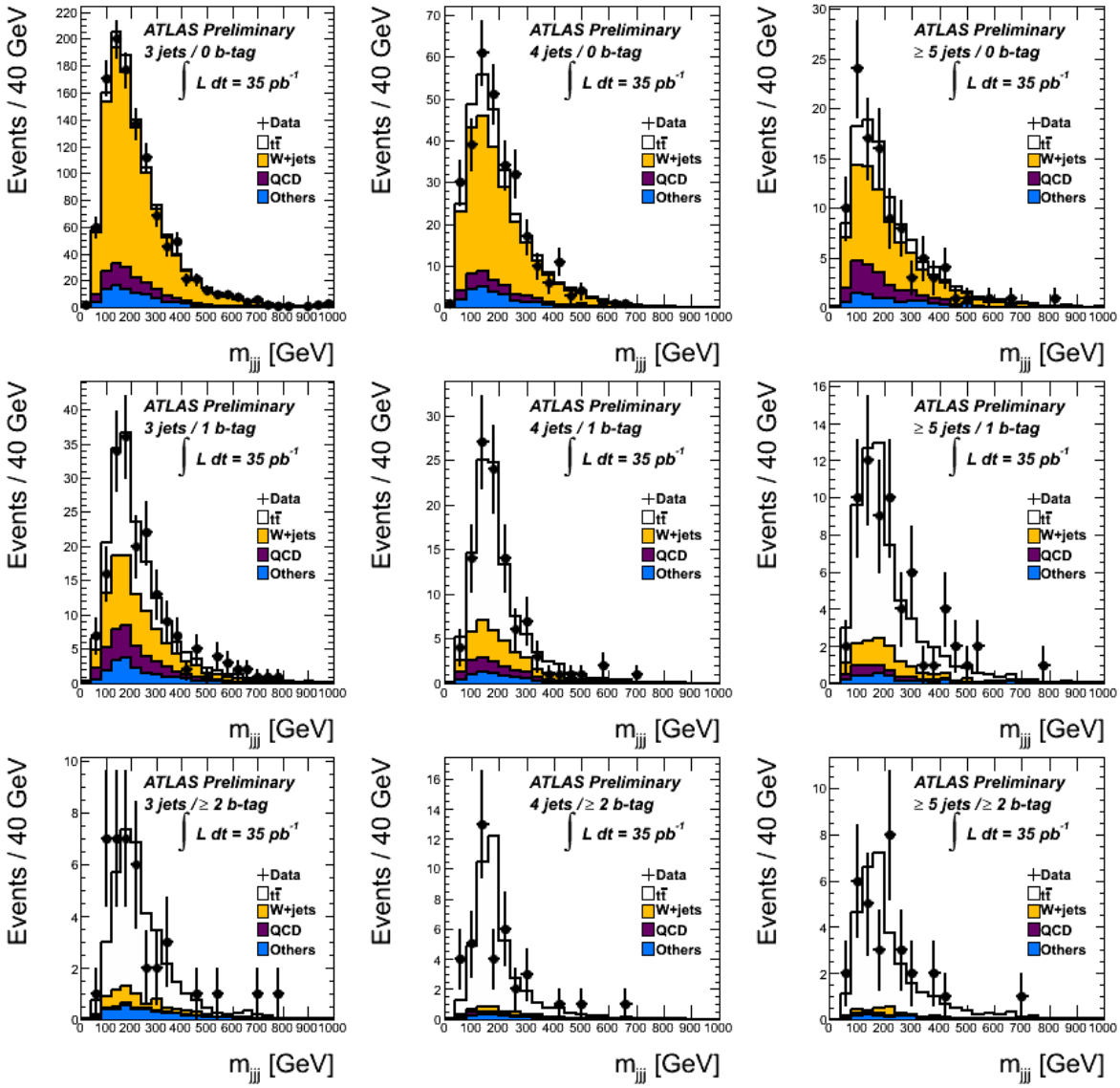

Figure 6: Top mass profile fit: result of the fit of the 3-jet invariant mass in the 3-, 4-, and ≥5-jet samples for the muon data. The $t\bar{t}$ and W+jets contributions have been scaled according to the results of the fit and the shapes of the Monte-Carlo samples morphed in accordance with the results of the nuisance factors.

7.3 Fit of kinematic variables in the 3- and ≥4-jet inclusive sample

In this approach referred to as the top mass standard fit, the hadronic top invariant mass m_{jjj} distribution is fitted simultaneously for events with zero, one, and at least two b-tags, using an unbinned extended likelihood procedure. Only events with at least three jets fulfilling the requirements of Section 3 are selected. The sample is split in events with exactly three jets and events with four or more jets. In the first sample there is only one possible jet combination to build m_{jjj}, whereas in the ≥ 4-jet bin an ambiguity arises in the assignment of the jets to the hadronic top quark. In this case, a kinematic fit is used to extract m_{jjj} at each event, reducing the combinatorial background in the mass distribution. The four jets with the highest transverse momenta are used in the event reconstruction. Constraints (Breit-

Wigner distributions) are applied to the two reconstructed W masses and to the two reconstructed top quark masses, the top pole mass being a free parameter. In addition to this parameter, 16 parameters are used in the fitting procedure: the energies of the 4 jets and of the lepton (p_{T} in the case of a muon), the azimuthal and longitudinal angles of the jets, and the three momentum components of the neutrino. The jet permutation that is the most consistent with originating from a $t\bar{t}$ event is kept.

The 3-jet and $\geq$ 4-jet samples are further split in three subsamples according to the number of b-tags: 0, 1 and 2 or more. Templates of m_{jjj} for the six cases are built from Monte-Carlo for the signal and from a QCD multi-jet enhanced data sample for the sum of all backgrounds. This analysis does not rely on the independent data-driven estimates of the QCD and W+jet backgrounds mentioned previously. It is a fully data-driven technique in which the shape of the hadronic top candidate invariant mass m_{jjj} for background is evaluated from data. A single template for both the QCD and the W+jet contributions is derived from a QCD-enriched data sample obtained by inverting some lepton identification cuts. The distributions are extracted from the $\geq$3 jet, 0-tag inclusive sample. The per-event b-tagging rate of events is fit together with the number of events for the background in the 2-jet data sample and extrapolated to the 3-jet sample using a correction factor obtained from Monte-Carlo simulation.

The fit to the distribution of the reconstructed hadronic top mass in the muon channel is shown in Fig. 7. The result of the fit in the electron channel is shown in Fig. C.1 in Appendix C. The measured $t\bar{t}$ cross-section, obtained by combining the electron and muon channels which are fitted separately, is $\sigma_{t\bar{t}} = 183 \pm 14\,(\mathrm{stat.})\,^{+20}_{-18}\,(\mathrm{syst.}) \pm 6\,(\mathrm{lumi})$ pb. This fit approach is less sensitive to the jet energy scale uncertainty (+3.8/-0.0%) and strongly constrains the b-tagging systematic uncertainty, which contributes $\pm$1.2% to the cross-section uncertainty. The most important contribution to the systematic uncertainty are heavy flavour content (6%) and ISR/FSR (4.5%). The fit also returns the b-tagging efficiency: 0.51 $\pm$ 0.03(stat.) $\pm$ 0.03(syst.), in excellent agreement with the expectations.

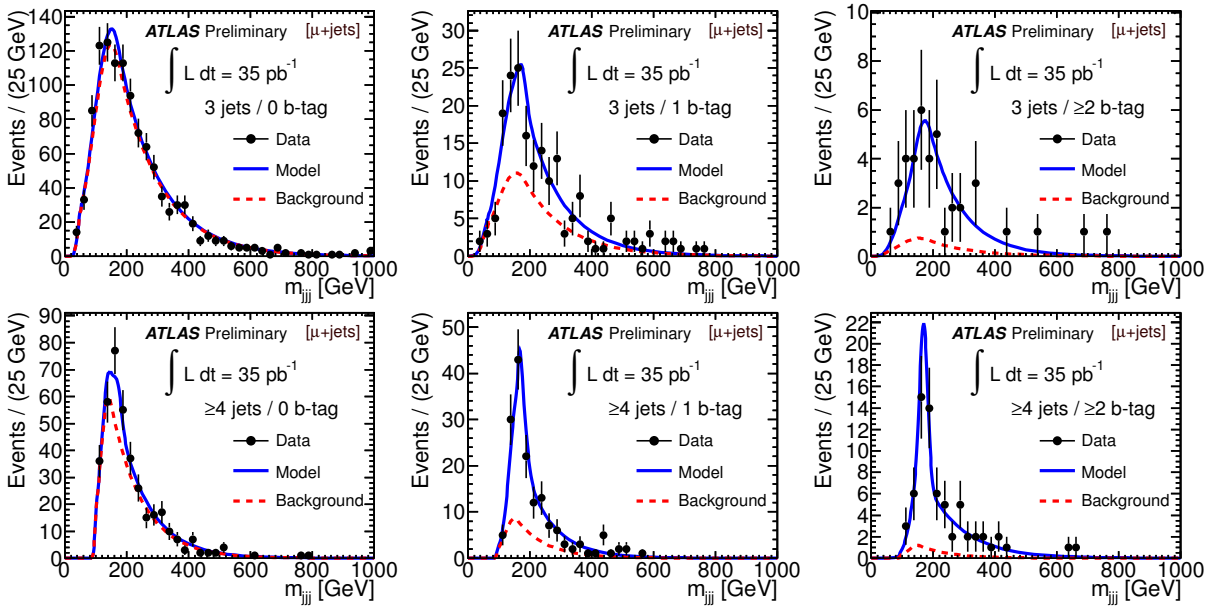

Figure 7: Top mass standard fit: fit to the distribution of reconstructed m_{jjj} in the 3- and $\geq$4-jet inclusive sample for the muon channel. Data are shown overlaid on the models for the background and the sum of signal and background. The upper row corresponds to the 3-jet bin and the bottom row to the $\geq$ 4-jet bin.

8 Summary

Measurements of the $t\bar{t}$ production cross-section in the single-lepton channel using the ATLAS detector and profiting from its b-tagging capabilities are reported. The cross-section is measured using a sample of 35 pb^{-1} with a profile likelihood fit to a discriminant variable. The result is

$$\sigma_{t\bar{t}} = 186 \pm 10\,(\text{stat.})^{+21}_{-20}\,(\text{syst.}) \pm 6\,(\text{lumi.})\,\text{pb}.$$

in good agreement with perturbative QCD calculations. The measurement is dominated by systematic uncertainties, the larger ones being the b-tagging calibration uncertainty and the understanding of the heavy flavour background.

Alternative measurements using different discriminant variables or extraction methods are also presented and agree with the main analysis. The summary of all the results is shown in Fig. 8 for the analyses discussed in Section 6 (multivariate), Section 7.2 (top mass profile fit), Section 7.3 (top mass standard fit), and Section 7.1 (counting method). Note that the measurements are correlated and should not be combined.

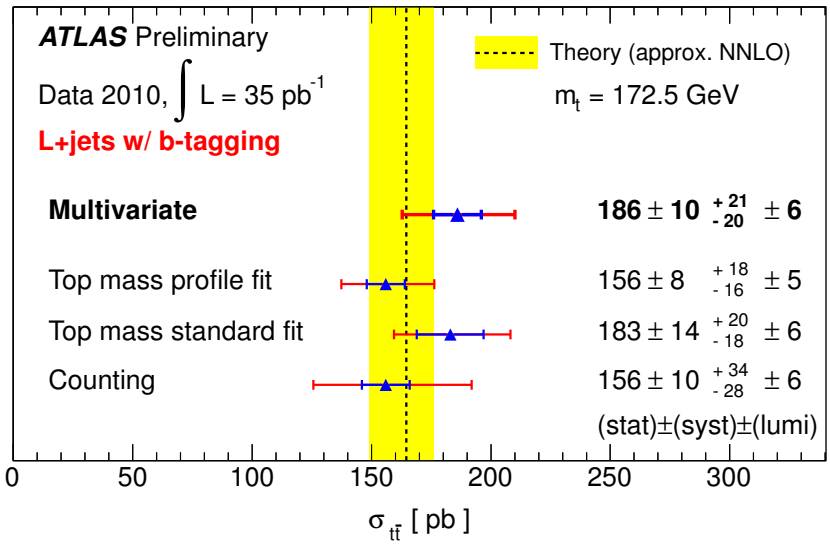

Figure 8: Summary of the $t\bar{t}$ cross-section measurements in the single-lepton channel with b-tagging using 35 pb^{-1} of data. Each measurement is quoted with its statistical, systematic and luminosity uncertainty. The yellow band corresponds to the theory uncertainty.

References

[1] The ATLAS Collaboration, G. Aad et al., *Measurement of the top quark-pair production cross-section with ATLAS in pp collisions at* $\sqrt{s}$ *= 7 TeV*, arXiv:1012.1792, to be published in Eur. Phys. J. **C**.

[2] S. Moch and P. Uwer, *Theoretical status and prospects for top-quark pair production at hadron colliders*, Phys. Rev. D78 (2008) 034003;
U. Langenfeld, S. Moch, and P. Uwer, *New results for $t\bar{t}$ production at hadron colliders*, Proc. XVII Int. Workshop on Deep-Inelastic Scattering and Related Topics, dx.doi.org/10.3360/dis.2009.131, arXiv:hep-ph/0907.2527;

M. Beneke et al., *Threshold expansion of the $gg(q\bar{q}) \rightarrow Q\bar{Q} + X$ cross section at $O(\alpha_s 4)$* , Phys. Lett. **B690** (2010) 483; Predictions in the paper are calculated with HATHOR [22] with $m_{\rm top}$ = 172.5 GeV, CTEQ66 [23], where PDF and scale uncertainties added linearly.

[3] The ATLAS Collaboration, G. Aad et al., *The ATLAS Experiment at the CERN Large Hadron Collider*, JINST 3 S08003 (2008).

[4] The ATLAS Collaboration, *Updated Luminosity Determination in pp Collisions at $\sqrt{s}$=7 TeV using the ATLAS detector*, ATLAS-COM-CONF-2011-011.

[5] S. Agostinelli et al., *GEANT4, a simulation toolkit*, Nucl. Instr. Meth. **A 506** (2003) 250.

[6] The ATLAS Collaboration, G. Aad et al., *The ATLAS Simulation Infrastructure*, Eur. Phys. J. **C 70** (2010) 823.

[7] M. Cacciari, G.P. Salam and G. Soyez, *The anti-k_t jet clustering algorithm*, JHEP **04** (2008) 063;
M. Cacciari and G. P. Salam, *Dispelling the N^3 myth for the k_t jet-finder*, Phys. Lett. **B 641** (2006) 57.

[8] The ATLAS Collaboration, G. Aad et al., *Measurement of inclusive jet and dijet cross-sections in proton-proton collisions at 7 TeV centre-of-mass energy with the ATLAS detector*, Eur. Phys. J. **C 71** (2011).

[9] The ATLAS Collaboration, *Performance of Impact Parameter-Based b-tagging Algorithms with the ATLAS Detector using Proton-Proton Collisions at $\sqrt{s}$= 7 TeV*, ATL-CONF-2010-091.

[10] The ATLAS Collaboration, *Performance of the ATLAS Secondary-Vertex b-tagging Algorithm in 7 TeV collision data*, ATL-CONF-2010-042.
The ATLAS Collaboration, *Calibrating the b-Tag and Mistag Efficiencies of the SV0 b-Tagging Algorithm in 3 pb^{-1} of Data with the ATLAS Detector*, ATL-CONF-2010-099.

[11] The ATLAS Collaboration, *Top Quark Pair Production Cross-section Measurements in ATLAS in the Single Lepton+Jets Channel without b-tagging*, ATLAS-CONF-2011-023.

[12] S. Frixione et al., *Single-top hadroproduction in association with a W boson*, JHEP 07 (2008) 029.

[13] J.M. Campbell and R.K. Ellis, *An update on vector boson pair production at hadron colliders*, Phys. Rev. D60 (1999) 113006.

[14] N. Reid and D.A.S. Fraser, *Likelihood Inference in the Presence of Nuisance Parameters*, in Proceedings of PHYSTAT 2003, *Statistical Problems in Particle Physics, Astrophysics, and Cosmology*, edited by L. Lyons, R.P. Mount, and R. Reitmeyer, (SLAC, Stanford, 2003), p. 265.

[15] M.L. Mangano et al., *ALPGEN, a generator for hard multiparton processes in hadronic collisions*, JHEP 07 (2003) 0013.

[16] B.P. Kersevan and E.Richter-Was, *The Monte Carlo Event Generator AcerMC version 3.5 with interfaces to PYTHIA 6.4, HERWIG 6.5 and ARIADNE 4.1*, arXiv:hep-ph/0405247.

[17] S. Frixione, P. Nason and B.R. Webber. *Matching NLO QCD and parton showers in heavy flavour production*, JHEP 08 (2003) 007, arXiv:hep-ph/0305252;
S. Frixione, E. Laenen and P. Motylinski, *Single-top production in MC@NLO*, JHEP 03 (2006) 092, arXiv:hep-ph/0512250.

[18] P. Nason, *A new method for combining NLO QCD with shower Monte Carlo algorithms*, JHEP 11546 (2004) 040.

[19] C. Corcella et al., *HERWIG 6.5: an event generator for Hadron Emission Reactions With Interfering Gluons (including supersymmetric processes)*, JHEP 01 (2001) 010, arXiv:hep-ph/0011363; G. Corcella et al., *HERWIG 6.5 release notes*, arWiv:hep-ph/0210213.

[20] *PYTHIA 6.4 physics and manual*, T. Sjstrand, S. Mrenna and P. Skands, JHEP05 (2006) 026.

[21] M. Botje et al., *The PDF4LHC Working Group Interim Recommendations*, arXiv:hep-ph/1101.0538.

[22] M. Aliev et al., *HATHOR HAdronic Top and Heavy quarks crOss section calculatoR*, Comput. Phys. Commun. **182** (2011) 1034.

[23] J. Pumplin et al., *New generation of parton distributions with uncertainties from global QCD analysis*, JHEP 07 (2002) 012.

Appendices

A Baseline analysis

Table A.1: Table of parameter values and their uncertainties as obtained from the fit. The first uncertainty value is the symmetric Hessian uncertainty from the second derivative of the log-likelihood function, and the second and third are the asymmetric uncertainties from scanning the likelihood function around the minimum. The nominal values of all fit parameters β_i are 1.0, the nominal values of all nuisance parameters δ_i are 0.0. The a-priori uncertainty on the nuisance parameters is 1.0.

Parameter	Value	Error	Error Up	Error Down
$\beta(t\bar{t})$	1.13	0.13	0.13	-0.12
β(W+jets) in μ+3 Jets	1.08	0.11	0.11	-0.11
β(W+jets) in μ+4 Jets	1.09	0.15	0.15	-0.14
β(W+jets) in μ+5 Jets	1.10	0.27	0.28	-0.26
β(W+jets) in e+3 Jets	1.04	0.14	0.14	-0.14
β(W+jets) in e+4 Jets	1.20	0.27	0.28	-0.24
β(W+jets) in e+5 Jets	0.95	0.33	0.34	-0.32
β(Z+jets)	1.07	0.31	0.31	-0.31
β(single t)	1.01	0.11	0.11	-0.11
β(diboson)	1.00	0.06	0.06	-0.06
β(QCD) in μ+3 Jets	0.51	0.41	0.41	-0.41
β(QCD) in μ+4 Jets	0.93	0.47	0.47	-0.47
β(QCD) in μ+5 Jets	0.74	0.44	0.45	-0.45
β(QCD) in e+3 Jets	1.03	0.48	0.49	-0.49
β(QCD) in e+4 Jets	0.99	0.50	0.50	-0.50
β(QCD) in e+5 Jets	0.97	0.49	0.49	-0.49
δ(b-tagging WP1)	-0.23	0.56	0.56	-0.54
δ(b-tagging WP2)	0.54	0.60	0.57	-0.62
δ(mistags WP1)	0.04	0.66	0.66	-0.64
δ(mistags WP2)	0.14	0.59	0.58	-0.57
δ(JES)	-0.52	0.40	0.42	-0.35
δ(Jet Efficiency)	-0.08	0.82	0.81	-0.83
δ(JER)	0.91	0.63	0.62	-0.63
δ(MC Generator (POWHEG+Herwig))	-0.21	0.56	0.57	-0.55
δ(Hadronization (POWHEG+Pythia))	-0.03	0.71	0.71	-0.71
$\delta(Wb\bar{b}/c\bar{c}$ Fraction)	-0.01	0.64	0.64	-0.65
$\delta(Wc$ Fraction)	-0.11	0.93	0.93	-0.93
δ(Pileup)	-0.22	0.58	0.59	-0.57
$\delta(\mu$ SFs)	-0.22	0.87	0.87	-0.76
$\delta(e$ SFs)	0.34	0.87	0.83	-0.89
$\delta(\mu$ Smearing)	-0.37	0.76	0.75	-0.73
$\delta(e$ Resolution)	-0.05	1.02	0.97	-0.97

B Fit of the 3-jet invariant mass in the 3-, 4-, and ≥ 5-jet samples

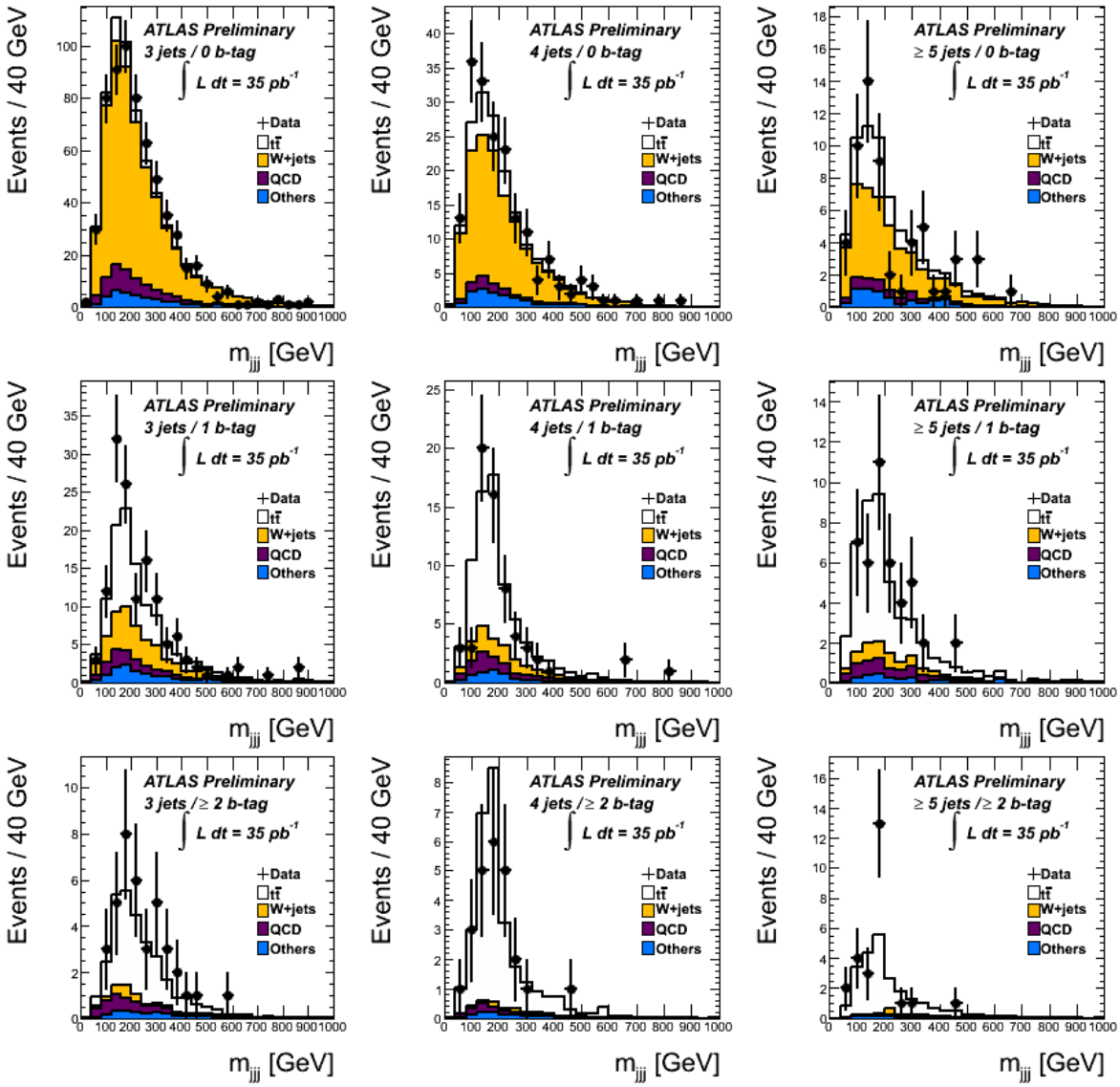

Figure B.1: Result of the fit of the 3-jet invariant mass in the 3-, 4-, and ≥5-jet samples for the electron data. The $t\bar{t}$ and W+jets contributions have been scaled according to the results of the fit and the shapes of the Monte-Carlo samples morphed in accordance with the results of the nuisance factors.

C Fit of kinematic variables in the 3- and ≥4-jet inclusive sample

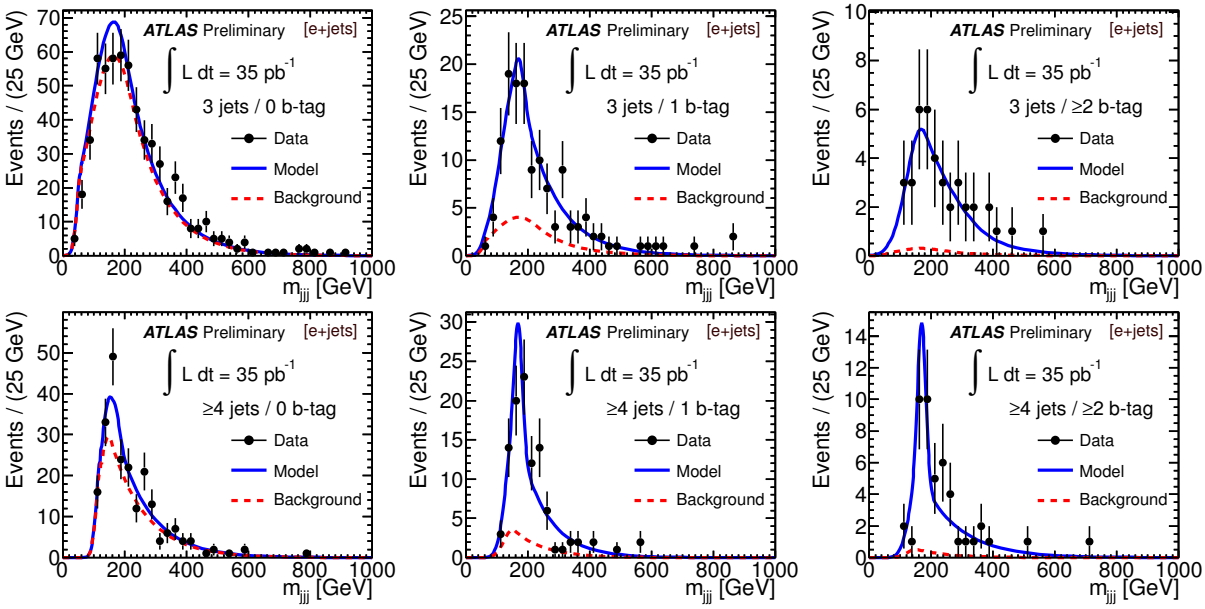

Figure C.1: Fit to the distribution of reconstructed m_{jjj} in the 3- and ≥4-jet inclusive sample for the electron channel. Data are shown overlaid on the models for the background and the sum of signal and background. The upper row corresponds to the 3-jet bin and the bottom row to the ≥ 4-jet bin.